Bioelectromagnetics 29:100–107 (2008)

Pulsed Electrical Stimulation for Control of Vasculature: Temporary Vasoconstriction and Permanent Thrombosis

Daniel Palanker,[1,2]* Alexander Vankov,[1,2] Yev Freyvert,[1,2] and Philip Huie[1,2]

[1]*Department of Ophthalmology, Stanford University School of Medicine, Stanford, California*

[2]*Hansen Experimental Physics Laboratory, Stanford University, Stanford, California*

A variety of medical procedures is aimed to selectively compromise or destroy vascular function. Such procedures include cancer therapies, treatments of cutaneous vascular disorders, and temporary hemostasis during surgery. Currently, technologies such as lasers, cryosurgery and radio frequency coagulation, produce significant collateral damage due to the thermal nature of these interactions and corresponding heat exchange with surrounding tissues. We describe a non-thermal method of inducing temporary vasoconstriction and permanent thrombosis using short pulse (microseconds) electrical stimulation. The current density required for vasoconstriction increases with decreasing pulse duration approximately as $t^{-0.25}$. The threshold of electroporation has a steeper dependence on pulse duration—exceeding $t^{-0.5}$. At pulse durations shorter than 5 μs, damage threshold exceeds the vasoconstriction threshold, thus allowing for temporary hemostasis without direct damage to surrounding tissue. With a pulse repetition rate of 0.1 Hz, vasoconstriction is achieved approximately 1 min after the beginning of treatment in both arteries and veins. Thrombosis occurs at higher electric fields, and its threshold increases with vessel diameter. Histology demonstrated a lack of tissue damage during vasoconstriction, but vascular endothelium was damaged during thrombosis. The temperature increase does not exceed 0.1 °C during these treatments. Bioelectromagnetics 29:100–107, 2008.

Key words: vasoconstriction; electrical stimulation; thrombosis; hemostasis; electroporation

INTRODUCTION

A variety of medical procedures seeks to selectively compromise or destroy vascular function. One such procedure is the treatment of solid tumors. Reduction in tumor blood perfusion reduces nutrient flow to the tumor and causes the accumulation of catabolite products and extracellular acidification, both of which result in a cascade of tumor cell death [Denekamp et al., 1983; Chaplin and Acker, 1987; Stratford et al., 1988].

One approach to creating vascular dysfunction involves inducing tumor-selective thrombosis to shut down the tumor's blood supply [Ran et al., 1998; Nilsson et al., 2001]. There are anticancer drugs and agents, including cytokines [Kallinowski et al., 1989; Naredi et al., 1993; Hill et al., 1995], which have been shown to cause such thrombosis. However, the effectiveness of these agents is often limited by the risk of systemic toxicity [Sersa et al., 1999] among other factors.

Various other therapies, including hyperthermia [Song, 1984], photodynamic therapy [Fingar and Henderson, 1987], and shock wave therapy [Gamarra et al., 1993] have also been shown to affect some degree of vascular dysfunction in tumors. However, complete and permanent hemostasis has yet to be achieved by these methodologies. Mechanical clamping of the tumor-supporting vasculature has also been proposed [Denekamp et al., 1983]; however, such a technique appears impractical due to the convoluted nature of tumor vasculature.

Selective destruction of vascular function can also be applied in the treatment of cutaneous vascular disorders such as telangiectasia (commonly known as ''spider veins'') and in the removal of cutaneous

Grant sponsors: NIH; Air Force Office of Scientific Research (MFEL Grant). Grant number: 2R01 EY012888-04.

*Correspondence to: Daniel Palanker, Stanford University, 452 Lomita Mall, Room 135, Stanford, CA 94305-4085.
E-mail: Palanker@stanford.edu

Received for review 21 February 2007; Final revision received 21 August 2007

DOI 10.1002/bem.20368
Published online 4 October 2007 in Wiley InterScience (www.interscience.wiley.com).

vascular lesions, for example, capillary hemangiomas (such as cafe-au-lait spots and port wine stains). These conditions all involve dilated or engorged cutaneous capillaries; while not often of physical concern, they can be unsightly and cause emotional distress in the patient.

The most common treatment for cutaneous vascular lesions is sclerotherapy, which entails the intravascular injection of one of a variety of agents into the abnormal blood vessels. The injected substance injures the interior walls of the capillary, causing it to shrink or disappear. Unfortunately, this treatment can be painful, only partially effective, and usually requires about one to 2 months before improvement can be seen. In addition, long-lasting side effects such as echymotic or hyperpigmented marks can occur.

Other treatments such as freezing, surgery, radiation, phototherapy, and laser therapy have also been employed for subcutaneous and cutaneous vascular conditions. Of these, laser therapy has been the most successful, as the destruction of the offending capillaries is achieved with minimal damage to the overlying skin [Lanigan, 2000]. Hemoglobin absorbs the laser light, and the resulting hyperthermia leads to the coagulation of blood within the outermost vessels. However, where the affected skin area is relatively deep, the superficial capillaries absorb most of the light energy and that which remains can be insufficient to treat the deeper vessels (referred to as ''shadowing''). This problem can be partially solved by the use of more penetrating wavelengths, but the reduced localization of heat in this case may necessitate longer and/or multiple treatments, which are both expensive and time-consuming. Additionally, laser therapy does not work as well with dark-skinned patients because the epidermal melanin absorbs a significant portion of the light, thus reducing the amount that reaches the blood. The increase in laser power that is required to compensate for such attenuation may lead to thermal injury and to post-inflammatory pigment changes of the skin.

Ostensibly, electrosurgery may be a viable alternative to the above-described modalities for treating tumors as well as cutaneous and subcutaneous vascular disorders. However, current electrosurgical devices and procedures rely on hyperthermia and tissue coagulation, and thus suffer from thermal damage not only to the target blood vessels but also to surrounding tissue.

Accordingly, there is still a need for improved methodologies for creating hemostasis within blood vessels without causing damage to adjacent tissue. In particular, there is a need for a more safe and effective way to treat vasculature in solid tumors, and vascular disorders both cutaneous and subcutaneous. In addition, temporarily reduced perfusion in vascular tissue would help to control bleeding during surgery, and would facilitate the coagulation of blood vessels, thus decreasing the amount of collateral thermal damage during electrocautery.

Thrombotic reaction of stagnated blood to direct electric current has been observed earlier [Hladovec, 1971, 1975]. Complete and permanent thrombosis in the rat artery has been achieved with a direct current of 2 mA applied to the mechanically clamped vessel for 5 min [Guarini, 1996]. This technique has not been applied to medical practice because mechanical clamping of multiple capillaries in a large area is impractical. Moreover, direct current causes gas formation on electrodes and electrochemical damage to tissue, which further precludes its therapeutic applications [Matsushima et al., 1994; Song et al., 1994; Xin et al., 1997].

The contractile response of blood vessels to monopolar electric current was observed with 100 μs pulses [Sersa et al., 1999]. However, the observed effect was only partial and transient.

In this article we describe the selective and non-thermal vascular effects of nanosecond-to-millisecond electric pulses that can induce complete temporary vasoconstriction or permanent thrombosis without direct damage to the surrounding tissue.

MATERIALS AND METHODS

Experiments were performed on chorioallantoic membranes (CAM) of chicken embryos in vivo during the second week (10–14 days) of incubation. The top air-filled portion of the egg shell was cracked and removed. The shell membrane was then peeled from the CAM, exposing the translucent vascularized chorioallantoic membrane, as described in detail in Leng et al. [2004]. The CAM was subsequently covered with a 4–5 mm layer of Dulbecco's phosphate buffered saline (DPBS) medium without Phenol Red (Catalog # 14287, Invitrogen, Carlsbad, CA). The medium was open to air, but not perfused and not oxygenated. All measurements were performed at room temperature. Most of the threshold measurements were performed with a glass pipette electrode of 1 mm exit diameter, filled with balanced salt solution medium (BSS, Alcon Laboratories, Fort Worth, TX) and positioned in contact with a target tissue, while a much larger (1 cm^2) return electrode was placed in the periphery of the egg. Pulses were generated by a homemade square voltage pulse generator operating in the mono-phasic and bi-phasic modes, within a voltage range of up to ±500 V. Voltage rise and fall time was 20 ns. The pulses of current followed the square shape of the voltage waveforms

on both electrodes with deviations not exceeding 5%. Voltage and current waveforms were measured using a digital oscilloscope (Tektronix TDS 3054), with current measured as a voltage drop across a 26 Ω resistor connected between the return electrode in the medium and the ground electrode of the pulse generator, as shown in Figure 1.

Threshold currents for vasoconstriction were determined for monophasic and biphasic electric pulses with durations varying from 100 ns to 10 ms. In these experiments, pulses were applied to arteries and veins of 100 μm in diameter for 5 min at a repetition rate of 0.1 Hz. The threshold of vasoconstriction was defined as a decrease in vessel diameter by at least a quarter (25%) during the first 10 seconds of stimulation. Threshold current for each pulse duration was averaged over five different eggs of the same age. In experiments with larger blood vessels, a 1 mm pipette was not sufficient, so we applied a Platinum foil electrode of 2 mm in length, 250 μm in width, and 50 μm in thickness, which was placed 0.5–1 mm above the tissue. About 50 eggs were used in vasoconstriction experiments.

Tissue damage in the vicinity of the pipette was assessed immediately after the treatment using a standard cell membrane permeability assay based on propidium iodide (PI) fluorescent dye (Sigma–Aldrich, St. Louis, MO) [Belloc et al., 1994; Wilde et al., 1994; Bevensee et al., 1995]. PI is normally a cell-impermeant molecule, and undergoes a 40-fold enhancement of fluorescence upon binding to nucleic acids. Thus, PI fluorescence of the cell nucleus indicates abnormal permeability of the cell membrane. Tissue fluorescence

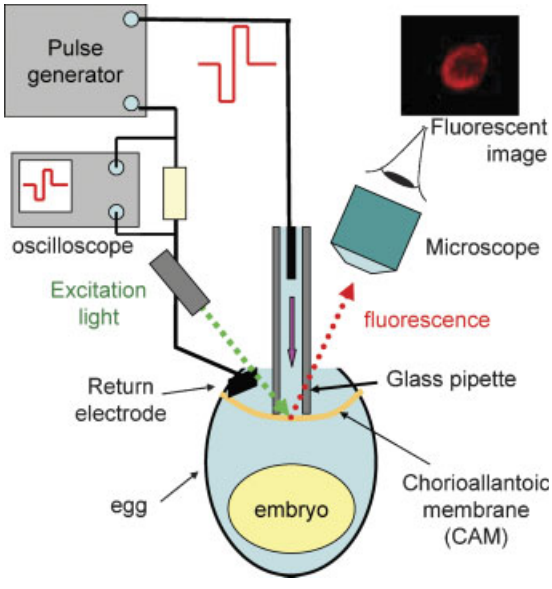

Fig. 1. Diagram of the experimental setup. [The color figure for this article is available online at www.interscience.wiley.com.]

assessment was achieved by means of a red blocking filter (Chroma, Rockingham, VT) positioned in front of the objective lens of the stereomicroscope (Leica MZ 9.5); excitation illumination was provided by a fiber-coupled Xenon lamp (OTI, XE-Lite, Toronto, Ontario) through a green excitation filter. PI was added to the medium prior to the treatment, and tissue fluorescence was assessed 15 min after its completion. Fluorescent images were taken with a stereomicroscope-mounted digital video camera (Toshiba IK-C43H 70).

Trials for the assessment of damaging current density levels on CAM were taken for up to 2 h on each tissue preparation while samples were kept at room temperature. During this period, the background fluorescence, measured in areas where tissues were not exposed to any electricity, remained low and the damage thresholds under identical settings remained constant. Tissue damage was determined by the appearance of a circular fluorescent pattern of similar size to the electrode diameter and brightness exceeding the background level by at least a factor of 2. Typically the fluorescence of the damaged tissue increased a couple of minutes after the treatment, but we allowed 15 min of delay for accurate determination near the threshold levels. For each pulse duration the current was increased until the PI fluorescence became detectable, using an untreated region of the tissue for every measurement. The current was initially increased by steps of 100% until the threshold was exceeded, and then decreased by steps of 20% for a more refined determination of the threshold level. The threshold current was then averaged over five sets of such measurements performed in different eggs. A total of about 200 eggs were used for measurements of the tissue damage threshold.

Cellular damage can result from the direct effects of the electric field (e.g., electroporation) or from the toxic products of electrochemical reactions at the metal-electrolyte interface. To eliminate the possibility of toxicity from the chemical by-products of the stimulation, the electrodes used in this study were encased in saline-filled glass pipettes. To prevent irreversible electrochemical reactions that can be caused by excessive current density on metal surfaces, the lead and return electrodes (made of Pt) had exposed areas significantly larger than the pipette exit aperture, and were placed far from the sample. The lead electrode was made from a multi-braided Pt wire exposed to saline inside the pipette over 10 mm of length. The return electrode was made of Pt foil of at least 50 mm^2 in area. Due to the large size of the metal electrodes inside and outside the pipette compared to the pipette aperture, the electrochemical potential drop at the metal surfaces was negligible, compared to the resistive voltage drop in

front of the aperture. Therefore, the pulse of current reproduced the square shape of the voltage pulse input; dividing the voltage by the measured current determined the impedance of the pipette. Pipette impedance was measured before each experiment to ensure the circuit was functional and the pipette tip was not blocked. The pipette was mounted on a three-dimensional micromanipulator to position the aperture against the surface of the tissue.

In the second set of experiments, threshold voltages for vasoconstriction and thrombosis were determined for arteries and veins of different sizes using 1 μs biphasic pulses (500 ns per phase) applied at a repetition rate of 1 Hz with exposures of up to 30 min. The status of blood vessels was then monitored for up to 24 h while the egg was incubated. For histological analysis, samples were fixed using glutaraldehyde–paraformaldehyde, embedded into araldite epoxy resin, sectioned into 1–2 μm thick sections, and stained with toluidine blue for light microscopy.

To assess the temperature rise during the treatment an electrode was placed close to the surface of the medium and temperature of water at the surface was measured using a thermal camera (ThermaCAM B20HS, FLIR Systems, Boston, MA).

RESULTS AND DISCUSSION

Typically, in small blood vessels (under 100 μm in diameter) vasoconstriction becomes detectable approximately 10 s after the beginning of stimulation, and increases during sustained treatment up to complete hemostasis, which is achieved approximately 3–5 min later. The rate of vasoconstriction did not significantly change with amplitude and repetition rate of the stimulating pulses: at highly super-threshold levels the starting time decreased to no shorter than 5 s. Approximately 30 s after the end of stimulation the vessels started dilating. Application of pulses at a repetition rate of 0.1 Hz was sufficient for maintaining hemostasis.

The typical appearance of complete vasoconstriction and thrombosis in CAM, as observed via surgical microscope, and the corresponding histological views of the vessels are shown in Figures 2 and 3, respectively. For better visibility these photographs have been taken from an area treated with the larger electrode (2 mm in length, 0.25 mm in width, and held 1 mm above the tissue). No noticeable damage to the tissue surrounding the constricted vessels could be seen. Figures 2a and 3a illustrate the appearance of the targeted vessel prior to the treatment. Figures 2b and 3b illustrate the vessel as it undergoes vasoconstriction during application of the electrical stimulation protocol. Clinical observation has demonstrated a complete stoppage of perfusion during fully developed vasoconstriction. However, fixation in formaldehyde leads to partial relaxation, so the blood vessel appears to be partially open in histological sections. When blood vessels were electrically stimulated at settings above the vasoconstriction threshold, but below the thrombosis threshold, they returned to their normal diameter approximately 1–3 min after the treatment terminated. Figures 2c and 3c depict thrombosis in the vessels under the electrode (electrode was removed for better visibility of the tissue underneath). The endothelium appears discontinuous and damaged. White blood cells are seen on the surface of the endothelium and necrotic endothelial cells are seen sloughed off the inner vessel wall; a thrombus is seen developing in the vessel lumen.

Figure 4 shows the relationship between the vasoconstriction threshold current density and the duration of the single monophasic (anodic) and biphasic (anodic first) pulses. As one can see in these graphs, the biphasic threshold is slightly higher than the monophasic threshold—by about 15% on average. Both curves can be approximated by a power function $\sim t^{-0.25}$. In Figure 5, thresholds of vasoconstriction and electroporation for monophasic (anodic) pulses are plotted as a function of pulse duration. The electroporation threshold scales more steeply with pulse duration: short-end asymptotes correspond to $t^{-0.7}$ for single pulses, $t^{-0.8}$ and $t^{-0.9}$ for pulses applied at a repetition rate of 0.1 and 1 Hz, respectively. Fitting curves shown in Figure 5 correspond to functions $a(1 + b/t)^c$, which exhibit power dependence at short pulse durations and a constant saturation level at long pulse durations. The theoretical model of electroporation [Joshi and Schoenbach, 2000] predicted such function with $c = 0.5$ for single pulses. However, the best fit of this function to our experimental data yielded $c = 0.7$. As one can see in Figure 5, at pulse repetition rate of 0.1 Hz tissue damage threshold exceeds the vasoconstriction threshold at pulse durations below 5 μs, so shorter pulses facilitate a non-damaging regime.

Thresholds of vasoconstriction and thrombosis for arteries and veins of three different sizes are summarized in Table 1. These results were obtained with biphasic (anodic first) pulses of 500 ns per phase applied at a repetition rate of 1 Hz. Because the rate of thrombosis varies with both the electric field and the size of the vessel, accurate determination of the threshold values required long exposures; 30 min treatments were used in these experiments, although at super-threshold values, thrombosis could be achieved in as few as 3 min. These experiments were performed with a platinum foil electrode of 2 mm in length,

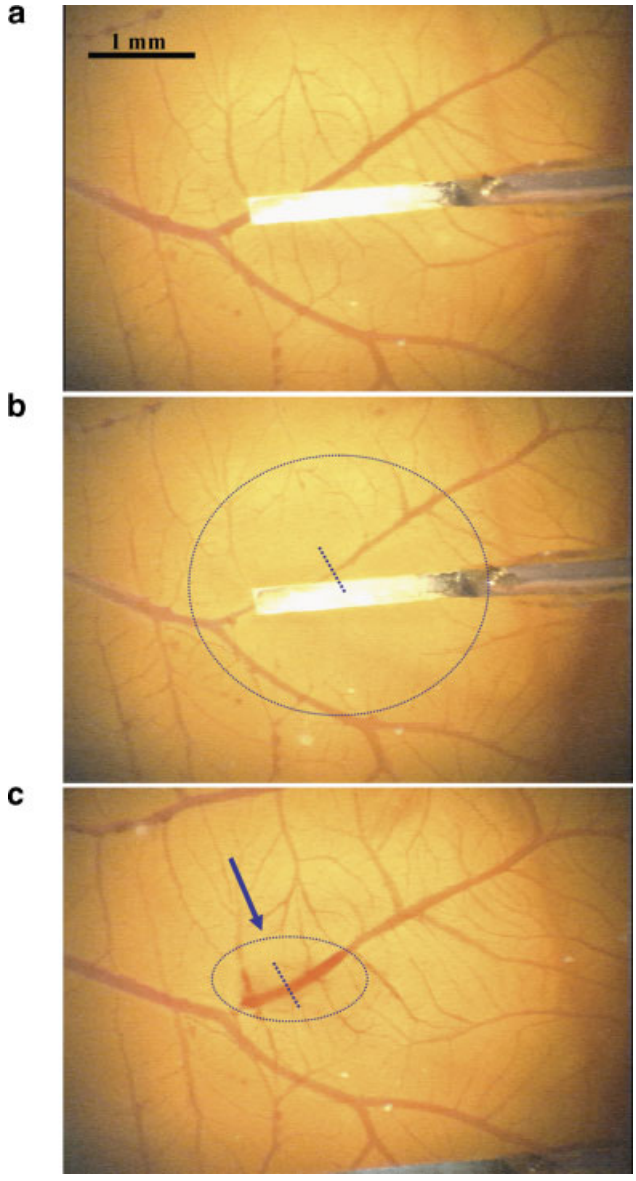

Fig. 2. Clinical appearance of the CAM, as observed via stereomicroscope. Scale bar shown in (a) is 1 mm. **a**: Normal appearance of CAM prior to treatment. Platinum foil electrode of 0.25 mm × 2 mm in size mounted at the end of a glass capillary is positioned just above the tissue. **b**: CAM and its blood vessels during the treatment. The large vessels are much less visible because of decreased blood flow. The area surrounding the vessels is blanched, indicating a lack of blood perfusion through the microcirculatory capillary bed. Dotted line represents the approximate cross-section of CAM shown in Figure 3b. **c**: CAM and its blood vessels after 15 min of treatment. The dotted line across a thrombus approximates location of the cross-section shown in Figure 3c. [The color figure for this article is available online at www.interscience.wiley.com.]

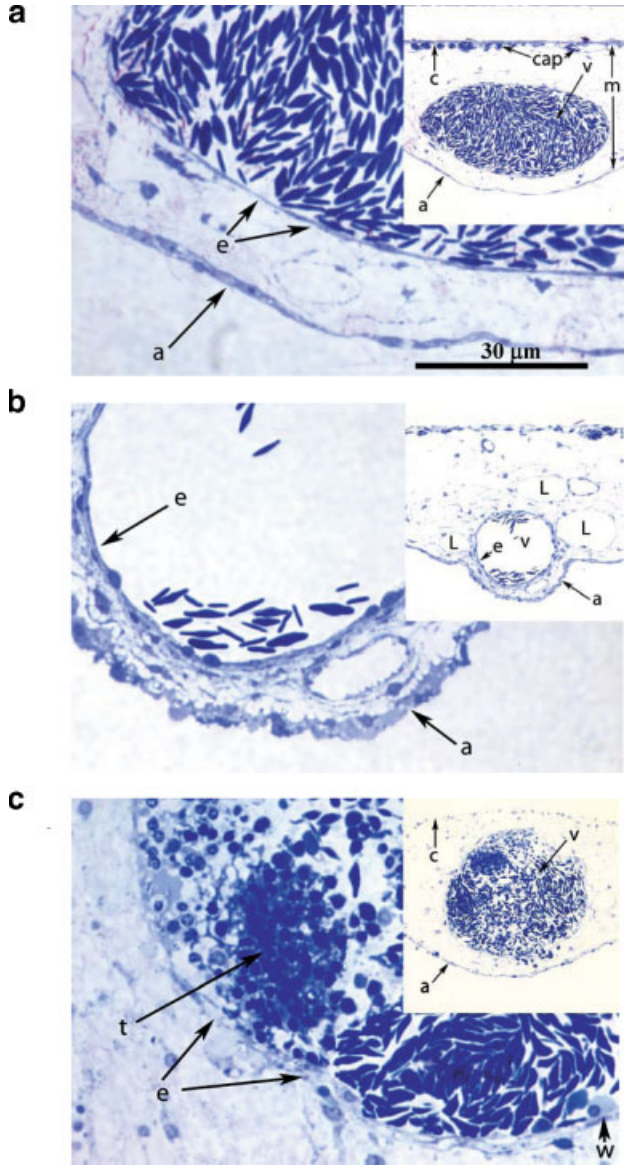

Fig. 3. Histological appearance of the CAM vein. Scale bar shown in (a) is 30 μm. **a**: Histology of CAM in untreated area, with chorionic (c) side up and allantoic (a) side down. Large vein (v) in the mesoderm (m) of the chorioallantoic membrane and thin walled capillaries (cap) just beneath the chorionic epithelium (c) are filled with red blood cells. Endothelium of blood vessels (e) and the blood cell morphology appear normal, having normal distribution and no thrombi. **b**: Histology of CAM at the point of vasoconstriction. The cross-sectional area of the vein (v) has dramatically decreased. The interstitial tissue surrounding the vessel and the allantoic epithelium (a) appear to be contracted. Small capillaries beneath the chorionic epithelium (cap) are void of blood. **c**: Histology of CAM at the thrombus area. The cross-sectional area of the vein (v) is similar to that of the vein shown in (a). There are areas of red blood cell aggregation and thrombosis (t). The endothelium (e) is damaged and discontinuous. White blood cells are seen on the surface of the endothelium (w). The interstium surrounding the vessel appears normal, and the allantoic epithelium (a) appears relaxed. [The color figure for this article is available online at www.interscience.wiley.com.]

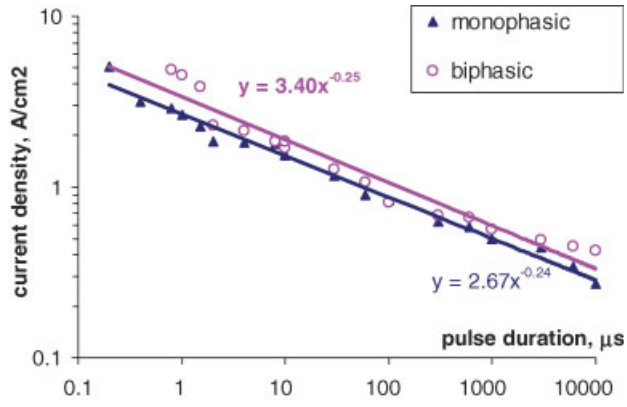

Fig. 4. Threshold current density for vasoconstriction of 100 µm blood vessels produced by monophasic (anodic, ▲) and bi-phasic (anodic-first, ○) pulses applied during 5 min at repetition rate of 0.1 Hz. Data are fit with a power function of $t^{-0.24}$ and $t^{-0.25}$ for monophasic and bi-phasic pulses, respectively. [The color figure for this article is available online at www.interscience.wiley.com.]

0.25 mm in width and 50 µm in thickness. Due to the non-uniform current density around elongated electrodes, (the electric field is enhanced at the edges) we express these results in units of electrode potential and total current rather than current density. The threshold voltage for vasoconstriction was higher for arteries (80 V) than for veins (60 V), and did not depend on the size of the vessels. However, the threshold of thrombosis increased approximately linearly with the vessel diameter

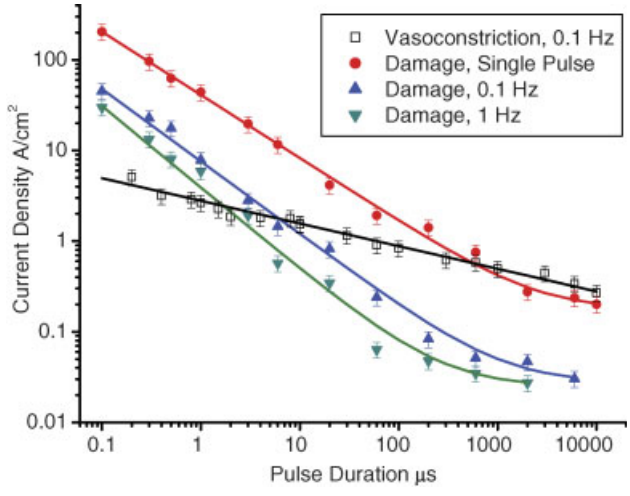

Fig. 5. Threshold values of current density at the exit of a 1 mm pipette required for inducing vasoconstriction (□) and tissue damage (●, ▲, ▼) using monophasic pulses of various durations. Vasoconstriction was produced during 5 min treatment at 0.1 Hz (□), while tissue damage thresholds have been measured for single pulses (●) and for a 5 min treatment at 0.1 Hz (▲) and 1 Hz (▼). Damage threshold data was fit with a function $f = a(1 + b/t)^c$, where $c = 0.7$ for single pulses, 0.8 and 0.9 for repetition rates of 0.1 and 1 Hz, respectively. [The color figure for this article is available online at www.interscience.wiley.com.]

for both arteries and veins. This phenomenon might allow for a selective treatment in which smaller vessels are permanently occluded while larger vessels experience only temporary vasoconstriction.

Average current density on the surface of the flat electrode (obtained by division of the total current by the electrode area 1 mm^2) is approximately an order of magnitude greater than current density obtained with the pipette electrodes. The reason for this difference is that the metal electrode was exposed on two sides, and was twice as long as the pipette diameter, so most of the current was injected away from the blood vessel. For example, at least half of the current is emitted from the upper surface of the electrode—away from the tissue, and much from the remote ends. For exactly these reasons we did not present the results in the units of average current density for metal foil electrode, as opposed to the pipette electrodes, where distribution of electric field is much better defined.

Values of the local electric field could be obtained by multiplying the local current density by the local tissue resistivity. Due to strong variability of the tissue resistivity between different layers and tissues, it requires very careful measurements using penetrating miroprobes. A lower estimate of the electric field could be made by multiplying the average current density by the resistivity of the physiological medium (saline, 70 Ω cm). For example, with a pulse duration of 1 µs, the threshold of vasoconstriction would correspond to 186 V/cm, and electroporation to 550 V/cm (at rep. rate of 0.1 Hz). However, the electric field inside the tissue is likely to exceed these levels due to higher tissue resistivity, especially in the epithelial layers.

Heating by electric current during several minutes of the treatment could affect the tissue if temperature is elevated by more than 10 °. Temperature rise during a short pulse can be estimated as follows: $\Delta T = tj^2\gamma/\rho c$, where j is the current density, t is the pulse duration, $\gamma = 70$ Ω cm (resistivity of the medium), $\rho = 1$ g/cm^3 (tissue density), and $c = 4.2$ J/(g K) is its heat capacity. For example, with $t = 1$µs and $j = 3$ A/cm^2 temperature rise $\Delta T = 0.15$ mK, while with $t = 10$ ms and $j = 0.3$ A/cm^2, $\Delta T = 15$ mK, which is far below the thermal damage threshold. Heat diffusion time τ across distance L can be estimated as: $\tau = L^2/4k$, where thermal diffusivity $k = 1.4 \times 10^{-7}$ m^2/s. For a 1 mm long electrode, τ is about 1 s. With pulse repetition rate of 0.1–1 Hz, heat will dissipate into the surrounding medium between pulses, so that the average temperature will not exceed the peak temperature at the end of each pulse.

To generate measurable temperatures during prolonged exposures we increased the repetition rate of the 0.5 µs pulses up to 300 Hz, and the voltage to

TABLE 1. Thresholds of Vasoconstriction and Thrombosis for Arteries and Veins of Various Sizes by Bi-Phasic Pulses of 1 μs in Duration Applied at Repetition Rate of 1 Hz During 30 min Via Electrode of 2 mm in Length, 0.25 mm in Width and 50 μm in Thickness

Vessel type	Vessel diameter, OD (μm)	Vasoconstriction threshold voltage (V)/current (A)	Thrombosis threshold voltage (V)/current (A)
Artery	75	80/0.37	90/0.41
Artery	100	80/0.37	170/0.75
Artery	225	80/0.37	300/1.3
Vein	75	60/0.28	90/0.41
Vein	150	60/0.28	120/0.54
Vein	275	60/0.28	250/1.1

At super-threshold values thrombosis could be achieved much faster—up to 3 min.

500 V. In these measurements, the electrode was placed close to the surface of liquid, and surface temperature was monitored using a FLIR infrared camera. We measured a temperature rise of 4.9 °C, which scaled linearly with the pulse repetition rate. Steady state temperature was reached within a few seconds, and stayed constant during the 5 min of treatment. Scaling this measurement to the maximal settings used in our experiments −300 V, 1 μs, 1 Hz, results in a temperature rise of 12 mK. Thus, no thermal damage should occur with a single pulse or with a sequence of pulses in the regimes applied in our experiments.

Two contractile cell types are found around the vessels in CAM. Smooth muscle cells surround large vessels, while pericytes surround arterioles in the mesodermal layer as well as smaller diameter capillaries and venules [Nico et al., 2004]. Both pericytes and smooth muscle cells contain contractile proteins and express similar ion channels [Sakagami et al., 1999; Bandopadhyay et al., 2001]. Pericytes are believed to regulate blood flow in microvasculature, while vascular smooth muscles regulate diameter of the larger vessels [Hirschi and D'Amore, 1996]. Vasoconstriction in CAM could be induced by calcium influx into the contractile cells surrounding the blood vessels [Resch et al., 2003]. When these cells are subjected to an electric field that is sufficient to open the voltage-sensitive ion channels, a net influx of extracellular calcium ions causes these cells to contract. It could also result from intracellular release of Ca ions from the sarcoplasmic reticulum. After the electric stimulation terminates, the affected vessels relax back to normal dimensions probably due to the reestablishment of baseline cytoplasmic calcium concentrations.

Thrombosis seems to be associated with damage to vascular endothelium by higher exposures to pulsed electric field. Endothelial damage normally results in the arrival of white blood cells and the activation of platelets to form a thrombus. This cascade also causes the vessel to relax, so after the stimulation terminates, the thrombus occludes the whole width of the blood vessel, as shown in Figures 2c and 3c.

The depth and lateral extent of electric field in the tissue can be controlled by the electrode geometry. For example, shallow penetration of electric field over a large area can be achieved by an array of alternating active and return electrodes, so that the distance between each pair determines the spatial extent of a dipole electric field. Such an array could be used to treat capillary hemangiomas—port wine stains.

CONCLUSIONS

Pulsed electrical stimulation can induce reversible vasoconstriction and permanent occlusion in arteries and veins. Heating of the tissue during this process is negligible, and with microsecond pulses, vasoconstriction can be produced below the threshold of electroporation. Thus, electronic control of vasculature can be performed without direct collateral damage to other cells in the tissue. The spatial extent of the electric field can be controlled by configuration of the electrode arrays to ensure proper tissue penetration depth. The maximal size of the permanently occluded vessels can be controlled by the applied voltage.

These phenomena could be applied to devascularize solid tumors, aneurysms, vascular malformations, and damaged vessels following trauma, as well as cutaneous and subcutaneous vascular conditions, such as port wine stains. They could also be used for temporary reduction of tissue perfusion during surgery to minimize bleeding, and thus help to reduce the extent of the thermal collateral damage zone due to coagulation.

REFERENCES

Bandopadhyay R, Orte C, Lawrenson JG, Reid AR, De Silva S, Allt G. 2001. Contractile proteins in pericytes at the blood–brain and blood–retinal barriers. J Neurocytol 30(1):35–44.

Belloc F, Dumain P, Boisseau MR, Jalloustre C, Reiffers J, Bernard P, Lacombe F. 1994. A flow cytometric method using hoechst 33342 and propidium iodide for simultaneous cell cycle analysis and apoptosis determination in unfixed cells. Cytometry 17(1):59–65.

Bevensee MO, Schwiening CJ, Boron WF. 1995. Use of bcecf and propidium iodide to assess membrane integrity of acutely isolated ca1 neurons from rat hippocampus. J Neurosci Methods 58(1–2):61–75.

Chaplin DJ, Acker B. 1987. The effect of hydralazine on the tumor-cytotoxicity of the hypoxic cell cytotoxin rsu-1069—Evidence for therapeutic gain. Int J Radiat Oncol Biol Phys 13(4):579–585.

Denekamp J, Hill SA, Hobson B. 1983. Vascular occlusion and tumor-cell death. Eur J Cancer Clin Oncol 19(2):271–275.

Fingar VH, Henderson BW. 1987. Drug and light dose dependence of photodynamic therapy—A study of tumor and normal tissue-response. Photochem Photobiol 46(5):837–841.

Gamarra F, Spelsberg F, Kuhnle GEH, Goetz AE. 1993. High-energy shock-waves induce blood-flow reduction in tumors. Cancer Res 53(7):1590–1595.

Guarini S. 1996. A highly reproducible model of arterial thrombosis in rats. J Pharmacol Toxicol Methods 35(2):101–105.

Hill SA, Sampson LE, Chaplin DJ. 1995. Antivascular approaches to solid tumor-therapy—Evaluation of vinblastine and flavone acetic-acid. Int J Cancer 63(1):119–123.

Hirschi KK, D'Amore PA. 1996. Pericytes in the microvasculature. Cardiovasc Res 32(4):687–698.

Hladovec J. 1971. Experimental arterial thrombosis in rats with continuous registration. Thrombosis Et Diathesis Haemorrhagica 26(2):407.

Hladovec J. 1975. Quantitative model of venous stasis thrombosis in rats. Physiol Bohemoslov 24(6):551–554.

Joshi RP, Schoenbach KH. 2000. Electroporation dynamics in biological cells subjected to ultrafast electrical pulses: A numerical study. Phys Rev E 62(1):1025–1033.

Kallinowski F, Schaefer C, Tyler G, Vaupel P. 1989. In vivo targets of recombinant human-tumor necrosis factor-alpha—Blood-flow, oxygen-consumption and growth of isotransplanted rat-tumors. Br J Cancer 60(4):555–560.

Lanigan SW. 2000. Lasers in dermatology. London: Springer. pp. 15–33.

Leng T, Miller JM, Bilbao KV, Palanker DV, Huie P, Blumenkranz MS. 2004. The chick chorioallantoic membrane as a model tissue for surgical retinal research and simulation. Retina—J Retinal Vitreous Dis. 24(3):427–434.

Matsushima Y, Takahashi E, Hagiwara K, Konaka C, Miura H, Kato H, Koshiishi Y. 1994. Clinical and experimental studies of anti-tumoral effects of electrochemical therapy (ect) alone or in combination with chemotherapy. Eur J Surgery 574:59–67.

Naredi PLJ, Lindner PG, Holmberg SB, Stenram U, Peterson A, Hafstrom LR. 1993. The effects of tumor-necrosis-factor-alpha on the vascular bed and blood-flow in an experimental rat hepatoma. Int J Cancer 54(4):645–649.

Nico B, Ennas MG, Crivellato E, Frontino A, Mangieri D, De Giorgis M, Roncali L, Ribatti D. 2004. Desmin-positive pericytes in the chick embryo chorioallantoic membrane in response to fibroblast growth factor-2. Microvasc Res 68(1): 13–19.

Nilsson F, Kosmehl H, Zardi L, Neri D. 2001. Targeted delivery of tissue factor to the ed-b domain of fibronectin, a marker of angiogenesis, mediates the infarction of solid tumors in mice. Cancer Res 61(2):711–716.

Ran S, Gao BN, Duffy S, Watkins L, Rote N, Thorpe PE. 1998. Infarction of solid Hodgkin's tumors in mice by antibody-directed targeting of tissue factor to tumor vasculature. Cancer Res 58(20):4646–4653.

Resch BE, Gaspar R, Falkay G. 2003. Application of electric field stimulation for investigations of human placental blood vessels. Obstet Gynecol 101(2):297–304.

Sakagami K, Wu DM, Puro DG. 1999. Physiology of rat retinal pericytes: Modulation of ion channel activity by serum-derived molecules. J Physiol 521(Pt 3):637–650.

Sersa G, Cemazar M, Parkins CS, Chaplin DJ. 1999. Tumour blood flow changes induced by application of electric pulses. Eur J Cancer 35(4):672–677.

Song CW. 1984. Effect of local hyperthermia on blood-flow and microenvironment—A review. Cancer Res 44(10):4721–4730.

Song YQ, Li CJ, Li YW, Song Q, Chang BP, Song LC, Liu CY, Wang T. 1994. Electrochemical therapy in the treatment of malignant-tumors on the body-surface. Eur J Surgery 574: 41–43.

Stratford IJ, Adams GE, Godden J, Nolan J, Howells N, Timpson N. 1988. Potentiation of the anti-tumor effect of melphalan by the vasoactive agent, hydralazine. Br J Cancer 58(2): 122–127.

Wilde GJ, Sundstrom LE, Iannotti F. 1994. Propidium iodide in vivo: An early marker of neuronal damage in rat hippocampus. Neurosci Lett 180(2):223–226.

Xin YL, Xue FZ, Ge BS, Zhao FR, Shi B, Zhang W. 1997. Electrochemical treatment of lung cancer. Bioelectromagnetics 18(1):8–13.